Int. J. Solids Structures Vol. 29, No. 22, pp. 2795–2814, 1992
Printed in Great Britain.

0020–7683/92 $5.00 + .00

ELASTIC–PLASTIC ANALYSIS OF COMBINED MODE I, II AND III CRACK-TIP FIELDS UNDER SMALL-SCALE YIELDING CONDITIONS

J. PAN
Department of Mechanical Engineering and Applied Mechanics, The University of Michigan, Ann Arbor, MI 48109, U.S.A.

and

C. F. SHIH
Division of Engineering, Brown University, Providence, RI 02912, U.S.A.

(*Received* 18 *June* 1990; *in revised form* 22 *March* 1992))

Abstract—Within the context of the small-strain approach, combined mode I, II and III near-tip fields of stationary cracks in power-law hardening materials are investigated. We use a finite element technique to obtain asymptotic angular stress solutions for combined mode I and II perturbed from mode III. These perturbation solutions with the same stress singularities as those of pure mode III are presented for different hardening materials. The perturbation results further suggest that the order of crack-tip stress singularities varies smoothly with changing mode mixity. We also employ full-field finite element computations to study the small-scale yielding near-tip fields for several combinations of prescribed remote mode I, II and III elastic K fields. These solutions verify an interesting pattern which agrees with the previous solutions for combined mode I and III loading as well as those for combined mode II and III loading: well within the plastic zone, under near mode I mixed-mode loadings, the in-plane stresses are slightly more singular than $r^{-1/(n+1)}$ while the out-of-plane shear stresses are slightly less singular than $r^{-1/(n+1)}$, where r is the radial distance to the tip and n is the strain hardening exponent of the material. To explain the complex behavior of the near-tip stresses, we introduce an effective in-plane shear stress and an effective out-of-plane shear stress to quantify the in-plane and out-of-plane plastic shear at different orientations in a consistent manner. The full-field solutions also corroborate the observation that the singularities of the in-plane stresses and the out-of-plane shear stresses vary smoothly with mode mixity.

1. INTRODUCTION

Asymptotic plane-strain and plane-stress crack-tip stress and strain fields for power-law hardening materials and perfectly plastic materials have been obtained under pure mode I and pure mode II conditions (Hutchinson, 1968a, b; Rice and Rosengren, 1968; Rice, 1968a) and under pure mode III conditions (Rice, 1968b). However, cracks in typical engineering structures are generally subject to combined mode I, II and III loading. Under combined mode I and II conditions the asymptotic crack-tip stress and strain fields for power-law hardening materials and perfectly plastic materials have been presented by Shih (1973, 1974). The results of Shih's full-field finite element computations indicate that within the plastic zone the mode I opening stress ahead of the tip is enhanced due to material plasticity. Further investigations of the material elasticity effects on combined mode I and II crack-tip fields for perfectly plastic materials can be found in Nemat-Nasser and Obata (1984), Saka *et al.* (1986) and Dong and Pan (1990a, b, c).

Within the small-scale yielding formulation, Pan and Shih (1990a, b) have obtained the near-tip fields by finite element methods under remote combined mode I and III K fields and under remote combined mode II and III K fields. Under combined mode I and III conditions the in-plane stresses well within the plastic zone are more singular than the HRR singularity while the out-of-plane shear stresses are less singular than the HRR singularity. In contrast, under combined mode II and III conditions, the in-plane stresses within the plastic zone are slightly less singular than the HRR singularity while the out-of-plane shear stresses are more singular than the HRR singularity. The qualitative nature and quantitative computational results of the angular and radial variations of both the in-plane stresses and the out-of-plane shear stresses agree well with those of the perturbation analysis of Pan (1990). This suggests that the perturbation analysis can clarify the nature of the crack-tip singularity under combined in-plane and out-of-plane shear loading conditions. It should

be noted that the separable stress function assumption for both in-plane and out-of-plane shear stresses in Pan (1990) are only valid when either the in-plane loading or the out-of-plane shear loading is smaller than the other, as shown in the finite element solutions of Pan and Shih (1990a, b) for their particular mode mixtures.

Based on the work by Pan and Shih (1990a, b) and Pan (1990), we make these observations regarding the structure of the combined mode I, II and III near-tip fields: under near mode I loading conditions the in-plane stresses should have a singularity stronger than that of the out-of-plane shear stresses, and under near mode II loading conditions the in-plane stresses should have a singularity weaker than that of the out-of-plane shear stresses. This leads to a question of the existence of the same singularity for both the in-plane stresses and the out-of-plane shear stresses asymptotically at the tip. The singularity must be the HRR singularity according to the J integral argument of Rice (1968) and Rice and Rosengren (1968). In this paper we investigate the asymptotic structure of crack-tip fields under combined mode I, II and III and attempt to answer the question of existence of the HRR singularity under combined mode I, II and III loading conditions by a perturbation analysis and full-field finite element computations.

We begin by reviewing an asymptotic analysis of combined mode I and II crack-tip fields perturbed from pure mode III as in Pan (1990). This leads to the first-order perturbed stress–strain relation for use in a finite element technique (Symington *et al.*, 1990) to obtain the solutions of the perturbed crack-tip fields. Perturbed combined mode I and II solutions with the HRR singularity are presented for different hardening exponents. These solutions yield the exact mode mixities where the in-plane stresses and the out-of-plane shear stresses have the same HRR singularity. Furthermore, the perturbation solutions suggest that the relative singularities of in-plane stresses to the out-of-plane shear stresses depend on mode mixity. Next we discuss several combined mode I, II and III full-field finite element solutions obtained under small-scale yielding conditions. These small-scale yielding solutions not only indicate that the crack-tip singularities for certain mixities of mode I, II and III are very close to the HRR singularity, but also point to some complex behavior of in-plane stresses under near mode I loading due to the dominant nature of mode I loading and plasticity. Finally we introduce an effective in-plane shear stress and an effective out-of-plane shear stress to quantify the in-plane and out-of-plane plastic shear at different orientations in a consistent manner.

2. HUTCHINSON–RICE–ROSENGREN (HRR) CRACK-TIP FIELDS

To describe the elastic–plastic behavior of the materials we consider here, we use the Ramberg–Osgood law, which is widely employed for fitting uniaxial tensile stress–strain relations:

$$\frac{\varepsilon}{\varepsilon_0} = \frac{\sigma}{\sigma_0} + \alpha\left(\frac{\sigma}{\sigma_0}\right)^n, \tag{1}$$

where ε is the tensile strain, σ is the tensile stress, ε_0 and σ_0 are the reference strain and reference stress (we take $\varepsilon_0 = \sigma_0/E$ where E is Young's modulus), α is a material constant and n is the hardening exponent. A generalization of eqn (1) gives the strains ε_{ij} written as the sum of an elastic part ε_{ij}^e and a volume-preserving plastic part ε_{ij}^p:

$$\varepsilon_{ij} = \varepsilon_{ij}^e + \varepsilon_{ij}^p. \tag{2}$$

The terms in (2) are given by

$$\varepsilon_{ij}^e = \frac{(1+\nu)}{E} s_{ij} + \frac{(1-2\nu)}{3E}\sigma_{kk}\delta_{ij},$$

$$\varepsilon_{ij}^p = \frac{3}{2}\alpha\left(\frac{\sigma_e}{\sigma_0}\right)^{n-1}\frac{s_{ij}}{\sigma_0}, \tag{3}$$

where ν is Poisson's ratio, s_{ij} ($= \sigma_{ij} - \frac{1}{3}\sigma_{kk}\delta_{ij}$) are the deviatoric stresses, and σ_e [$= (3s_{ij}s_{ij}/2)^{1/2}$] is the effective stress.

We consider a crack in a Ramberg–Osgood solid, as shown in Fig. 1, where r and θ are the polar coordinates centered at the crack tip. As r approaches 0, the linear elastic part of the strain is negligible compared to the plastic part. The asymptotic crack-tip stress, strain and displacement fields can then be expressed as (Hutchinson, 1968a, b; Rice and Rosengren, 1968; Rice, 1968b; Shih, 1973, 1974)

$$\sigma_{ij} = \sigma_0 \left(\frac{J}{\alpha \sigma_0 \varepsilon_0 I r} \right)^{1/(n+1)} \tilde{\sigma}_{ij}(\theta; n, M),$$

$$\varepsilon_{ij} = \alpha \varepsilon_0 \left(\frac{J}{\alpha \sigma_0 \varepsilon_0 I r} \right)^{n/(n+1)} \tilde{\varepsilon}_{ij}(\theta; n, M),$$

$$u_i - \hat{u}_i = \alpha \varepsilon_0 r \left(\frac{J}{\alpha \sigma_0 \varepsilon_0 I r} \right)^{n/(n+1)} \tilde{u}_i(\theta; n, M), \tag{4}$$

where the dimensionless constant I and the dimensionless angular functions $\tilde{\sigma}_{ij}$, $\tilde{\varepsilon}_{ij}$, and $\tilde{u}_i$ depend upon the hardening exponent n; the state of plane-strain, plane-stress or anti-plane deformation; and the mode parameter M (mode I, mode II, mixed-mode I and II, or mode III). The constants $\hat{u}_i$ allow for a possible rigid body motion of the crack tip itself. The J integral (Rice, 1968a) in eqn (4) represents the amplitude of the singular crack-tip stress and strain fields. Recent studies of the asymptotic crack-tip fields for power-law hardening orthotropic materials and for power-law hardening pressure-sensitive dilatant materials show the same type of functional forms as eqn (4) for the asymptotic crack-tip fields (Pan and Shih, 1986, 1988; Li and Pan, 1990a, b).

Under combined mode I, II and III conditions, eqn (4) may not accurately represent the fields within physically reasonable radial distances to the tip for all mode mixtures since in general the relative singularities of the in-plane stresses and the out-of-plane shear stresses depend on the radial distance r to the tip. For the convenience of quantification, three plastic mixity factors $M^p_{13}(r)$, $M^p_{23}(r)$ and $M^p_{12}(r)$ can be defined from the ratios of the in-plane opening stress $\sigma_{\theta\theta}$, the in-plane shear stress $\sigma_{r\theta}$, and the out-of-plane shear stress $\sigma_{\theta z}$ at a distance r ahead of the tip as

$$M^p_{13}(r) = \frac{2}{\pi} \tan^{-1} \left[\frac{\sigma_{\theta\theta}(r, \theta = 0)}{\sigma_{\theta z}(r, \theta = 0)} \right], \tag{5}$$

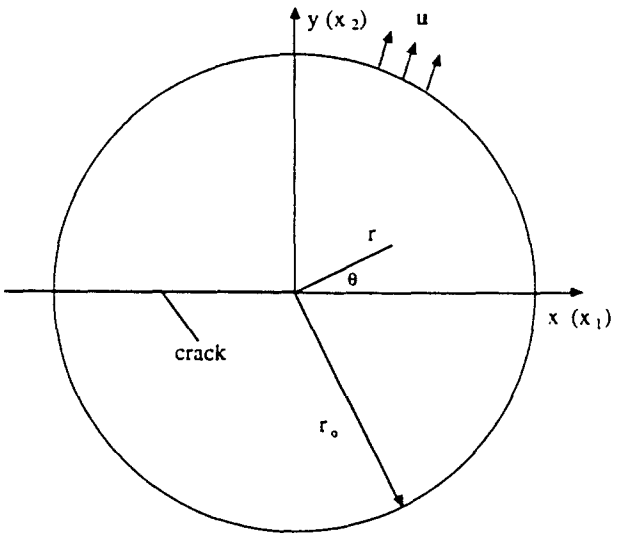

Fig. 1. A crack subjected to combined mode I, II and III elastic K fields along the circumferential boundary.

$$M^{\sigma}_{23}(r) = \frac{2}{\pi}\tan^{-1}\left[\frac{\sigma_{rr}(r,\theta=0)}{\sigma_{zz}(r,\theta=0)}\right], \tag{6}$$

and

$$M^{\sigma}_{12}(r) = \frac{2}{\pi}\tan^{-1}\left[\frac{\sigma_{\theta\theta}(r,\theta=0)}{\sigma_{rr}(r,\theta=0)}\right]. \tag{7}$$

Here r is smaller than the smallest radial extent of the plastic zone. Thus, when both M^{σ}_{13} and M^{σ}_{23} equal 0, we have pure mode III crack-tip fields. Under pure in-plane loading conditions, both M^{σ}_{13} and M^{σ}_{23} equal 1. We need only the mixity factor $M^{\sigma}_{12}(r)$ (Shih, 1973, 1974) to specify the mixed mode I and II crack-tip field. The asymptotic crack-tip fields exist under in-plane mixed-mode conditions (Shih, 1973, 1974): an asymptotic value of $M^{\sigma}_{12}(r)$ as r approaches 0 (within a physically reasonable radial distance to the tip) can be found under small-scale yielding. The values of $M^{\sigma}_{13}(r)$, $M^{\sigma}_{23}(r)$ and $M^{\sigma}_{12}(r)$ range between 1 and 0 for combined mode I, II and III near-tip fields. Note that only two of the three mode mixities are needed to specify a combined mode I, II and III crack-tip field at a given radial distance r.

3. PERTURBATION ANALYSIS AND RESULTS

In this section, the perturbation analysis of Pan (1990) which leads to the essential information for the modification of Symington *et al.*'s (1990) finite element method for calculation of the perturbed asymptotic crack-tip fields is briefly discussed. The in-plane stress function ϕ and the out-of-plane stress function ψ are assumed in separable forms as in Pan (1990):

$$\phi = Kr^{s}\tilde{\phi}(\theta) \tag{8}$$

and

$$\psi = Lr^{t}\tilde{\psi}(\theta), \tag{9}$$

where K, L, s and t are constants, and $\tilde{\phi}(\theta)$ and $\tilde{\psi}(\theta)$ are functions of their argument θ for a given power-law hardening material. The stresses derived from the stress functions are

$$\begin{aligned}
\sigma_{rr} &= Kr^{s-2}\tilde{\sigma}_{rr},\\
\sigma_{\theta\theta} &= Kr^{s-2}\tilde{\sigma}_{\theta\theta},\\
\sigma_{r\theta} &= Kr^{s-2}\tilde{\sigma}_{r\theta},\\
\sigma_{rz} &= Lr^{t-2}\tilde{\sigma}_{rz},\\
\sigma_{\theta z} &= Lr^{t-2}\tilde{\sigma}_{\theta z},
\end{aligned} \tag{10}$$

where

$$\begin{aligned}
\tilde{\sigma}_{rr} &= s\tilde{\phi} + \tilde{\phi}'',\\
\tilde{\sigma}_{\theta\theta} &= s(s-1)\tilde{\phi},\\
\tilde{\sigma}_{r\theta} &= (1-s)\tilde{\phi}',\\
\tilde{\sigma}_{rz} &= \tilde{\psi}',\\
\tilde{\sigma}_{\theta z} &= (1-t)\tilde{\psi}.
\end{aligned} \tag{11}$$

Here $(\,)'$ represents $\partial(\,)/\partial\theta$. Note that for a given power-law hardening material, $\tilde{\sigma}_{rr}$, $\tilde{\sigma}_{\theta\theta}$, and $\tilde{\sigma}_{r\theta}$ are functions of θ and s, and $\tilde{\sigma}_{rz}$ and $\tilde{\sigma}_{\theta z}$ are functions of θ and t. As shown in

Hutchinson (1968a, b), Rice and Rosengren (1968), Shih (1973, 1974) and Rice (1968b), the value of s and t is

$$s = t = \frac{2n+1}{n+1} \tag{12}$$

for either pure in-plane modes (mode I, mode II and combined mode I and II) or a pure out-of-plane shear mode (mode III). When we seek solutions of the singular crack-tip fields of the forms (10) and (11) under combined in-plane and out-of-plane shear loading conditions, the values of s and t in general are assumed to be different. Since we are seeking singular solutions in the immediate vicinity of the crack tip, we are interested in the solutions with both s and t being less than 2. As r approaches 0, the in-plane mode will dominate for $s < t$ whereas the out-of-plane shear mode will dominate for $t < s$. Remember that the assumptions of (8) and (9) are approximately valid when either the in-plane mode or the out-of-plane shear mode is smaller than the other for the mode mixtures investigated by Pan and Shih (1990a, b).

The coupling of the in-plane plastic deformation and out-of-plane shear plastic deformation is through the effective stress σ_e in the constitutive equation (3). The effective stress σ_e in the cylindrical coordinate system is expressed as

$$\sigma_e^2 = \tfrac{3}{4}(\sigma_{rr} - \sigma_{\theta\theta})^2 + 3\sigma_{r\theta}^2 + 3\sigma_{rz}^2 + 3\sigma_{\theta z}^2. \tag{13}$$

Substituting (10) into (13) gives

$$\sigma_e^2 = (Kr^{s-2})^2 \tilde{S}_e^2 + (Lr^{t-2})^2 \tilde{T}_e^2, \tag{14}$$

where

$$\tilde{S}_e^2 = \tfrac{3}{4}(\tilde{\sigma}_{rr} - \tilde{\sigma}_{\theta\theta})^2 + 3\tilde{\sigma}_{r\theta}^2 \tag{15}$$

and

$$\tilde{T}_e^2 = 3\tilde{\sigma}_{rz}^2 + 3\tilde{\sigma}_{\theta z}^2. \tag{16}$$

Note that $\tilde{S}_e$ and $\tilde{T}_e$ are functions of θ for a given n. More importantly, since we assume that s is not equal to t, σ_e cannot be expressed as a separable function of r and θ, such as those stresses in (10). We can define the maximum magnitude of the θ-variations $\tilde{S}_e$ and $\tilde{T}_e$ to be unity. Then K and L represent the singularity amplitudes of the in-plane stresses and the out-of-plane shear stresses, respectively.

It is possible that the values of s and t are equal to each other for certain mode mixities. When $s = t$ the asymptotic governing equations can be derived and then supposedly solved by the shooting method. However, the shooting method will be cumbersome and difficult for solving this class of problems with homogeneous stress-free boundary conditions as discussed in Shih (1973, 1974), especially for combined mode I, II and III problems. It is also possible that we try to solve for perturbed mode III crack-tip fields from combined mode I and II solutions. However, the simplest task is to solve for perturbed combined mode I and II crack-tip fields from mode III since closed-form mode III crack-tip stress solutions exist (Rice, 1968b). Therefore we consider the cases where the contribution of the in-plane stresses to the effective stress is smaller than that of the out-of-plane shear stresses (or $K/L \ll 1$). Equation (14) can be rewritten as

$$\sigma_e = Lr^{t-2}\tilde{\sigma}_e, \tag{17}$$

where $\tilde{\sigma}_e$ is now defined as

$$\tilde{\sigma}_e^2 = \tilde{T}_e^2 \left(1 + \left(\frac{K}{L}\right)^2 r^{2(s-t)} \frac{\tilde{S}_e^2}{\tilde{T}_e^2}\right). \tag{18}$$

As shown in the finite element computations of Pan and Shih (1990a, b), the singularities of the crack-tip in-plane stresses and out-of-plane shear stresses usually differ only slightly. Therefore, $s-t$ in (18) can be assumed to be a small number. For small r, $r^{2(t-s)}$ in (18) becomes finite and has an order of unity. Therefore, $\tilde{\sigma}_e$ does have a weak dependence on r. Then, $(K/L)^2$ determines the order of magnitude of the second term on the right-hand side of (18). Note that $(K/L)^2 r^{2(s-t)}$ represents a mixity factor of the in-plane mode and the out-of-plane shear mode.

The strains can be expressed as

$$\begin{aligned}
\varepsilon_{rr} &= N\left(\frac{K}{L}\right) r^{n(t-2)+s-t} \tilde{\sigma}_e^{n-1} \tfrac{1}{2}(\tilde{\sigma}_{rr} - \tilde{\sigma}_{\theta\theta}),\\
\varepsilon_{\theta\theta} &= -\varepsilon_{rr},\\
\varepsilon_{r\theta} &= N\left(\frac{K}{L}\right) r^{n(t-2)+s-t} \tilde{\sigma}_e^{n-1} \tilde{\sigma}_{r\theta},\\
\varepsilon_{rz} &= N r^{n(t-2)} \tilde{\sigma}_e^{n-1} \tilde{\sigma}_{rz},\\
\varepsilon_{\theta z} &= N r^{n(t-2)} \tilde{\sigma}_e^{n-1} \tilde{\sigma}_{\theta z},
\end{aligned} \tag{19}$$

where

$$N = \left(\frac{3}{2}\right)\alpha\left(\frac{L}{\sigma_0}\right)^n. \tag{20}$$

Under pure mode III conditions, the closed-form stress solutions given by Rice (1968b) are

$$\tilde{T}_e = \left[\frac{n+1}{2n}\frac{\sin 2\eta}{\sin\theta}\right]^{1/(n+1)}, \tag{21}$$

where

$$2\eta = \theta + \sin^{-1}\left[\frac{n-1}{n+1}\sin\theta\right]. \tag{22}$$

Note that $\tilde{T}_e(0) = 1$ and the value of t equals the HRR value for pure mode III.

When we consider the asymptotic combined mode I and II crack-tip fields perturbed from mode III, the lowest order relation between the normalized in-plane strains $\tilde{\varepsilon}_{ij}$ and the normalized in-plane stresses $\tilde{\sigma}_{ij}$ in matrix form is

$$\begin{Bmatrix} \tilde{\varepsilon}_{rr} \\ \tilde{\varepsilon}_{\theta\theta} \\ 2\tilde{\varepsilon}_{r\theta} \end{Bmatrix} = \tfrac{1}{2}\tilde{T}_e^{n-1}\begin{pmatrix} 1 & -1 & 0 \\ -1 & 1 & 0 \\ 0 & 0 & 4 \end{pmatrix}\begin{Bmatrix} \tilde{\sigma}_{rr} \\ \tilde{\sigma}_{\theta\theta} \\ \tilde{\sigma}_{r\theta} \end{Bmatrix}. \tag{23}$$

Note that $\tilde{T}_e$ is a function of θ for a given power-law hardening material. Equation (23) is the essential input for employing Symington *et al.*'s (1990) finite element method to solve for the perturbed asymptotic crack-tip fields.

Symington *et al.* (1990) constructed a finite element method for computing the angular variation of asymptotic singular crack-tip stresses and strains. In their formulation the asymptotic stress and strain fields must be of a separable form in polar coordinates. The radial dependence of stresses and strains is assumed to be known. Their finite element method is based on a weak form of the compatibility equation with the homogeneous boundary conditions at the stress-free crack faces. We adopt their method to calculate the

perturbed crack-tip fields. Here we only present the necessary modification of their finite element method in eqn (23) for the present perturbation problem. Interested readers are referred to Symington *et al.* (1990) for the detailed finite element formulation. Under combined mode I and II loading, the stress and strain singularities [denoted by β and ρ in Symington *et al.* (1990)] are known from the J integral argument by Rice (1968b) and Symington *et al.* (1990) actually solved a system of nonlinear equations using the Newton–Raphson method.

For the present perturbation problem, the compliance matrix between the normalized in-plane strains $\tilde{\varepsilon}_{ij}$ and the normalized in-plane stresses $\tilde{\sigma}_{ij}$ in eqn (23) is a function of the angular location θ only. Here, $\beta = 2-s$ and $\rho = t-s-n(t-2)$ where the value of t of unperturbed pure mode III is the HRR value. The value of s depends upon the in-plane mode mixity. Inversely, the in-plane mode mixity depends upon the value of s. If a value of s is given, then the system of governing equations based on the formulation of Symington *et al.* (1990) with eqns (23) becomes linear and no iteration is required to solve for the angular variation of the perturbed asymptotic crack-tip fields. In other words, for a given value of s, the finite element computation will result in an angular variation of stresses with a mode mixity evaluted at $\theta = 0$.

The finite element model of the domain from $-\pi$ to π is constructed by 360 2-node elements with Hermitian interpolation functions. Discussions of the mesh refinement on computational results can be found in Symington *et al.* (1990). The values of s for input to the finite element calculations were selected from the solutions of perturbed mode I and mode II by Pan (1990). The finite element results agree well with those obtained by the shooting method. Next we used values of s between those for perturbed mode I and mode II. For these values of s we obtained solutions with the mode mixity factors M_{12}^{p} ranging from 1 for perturbed mode I and 0 for perturbed mode II. In the interest of space we present the combined mode I and II solutions with the HRR singularity for $n = 3$ and $n = 10$ in Fig. 2. The values of M_{12}^{p} for the perturbed crack-tip fields with the HRR singularity shown in Fig. 2 are 0.56 and 0.46 for $n = 3$ and $n = 10$, respectively. The value of M_{12}^{p} for the perturbed crack-tip fields with the HRR singularity is 0.38 for $n = 20$. Observe that the mode mixity for the perturbed crack-tip field with the HRR singularity decreases with the increase of the hardening exponent n. This is qualitatively in agreement with the general trend that the enhancement of the in-plane opening stress increases with the increase of n under both combined mode I and II conditions and combined mode I and III conditions. Note that $\tilde{\sigma}_{rr}$ at 180° and -180° has the same magnitude. A simple perturbation of the analysis in Budiansky and Rice (1973) can indicate that the perturbed radial stresses at the stress-free crack faces must have the same magnitude but not necessarily the same sign.

4. SMALL-SCALE YIELDING COMPUTATIONAL MODEL

We consider the small-scale yielding problem depicted in Fig. 1, where a crack in a circular domain is shown. Along the remote circular boundary, displacement fields based on the mode I, and II and III asymptotic crack-tip solutions for linear elastic materials are applied. The in-plane displacements u_i $(i = 1, 2)$ and the out-of-plane displacement u_3 are prescribed as

$$u_i = \frac{K_{\mathrm{I}}}{2G}\left(\frac{r}{2\pi}\right)^{1/2}\tilde{u}_i^{\mathrm{I}}(\theta, \nu) + \frac{K_{\mathrm{II}}}{2G}\left(\frac{r}{2\pi}\right)^{1/2}\tilde{u}_i^{\mathrm{II}}(\theta, \nu), \tag{24}$$

and

$$u_3 = \frac{K_{\mathrm{III}}}{2G}\left(\frac{r}{2\pi}\right)^{1/2}\tilde{u}_3^{\mathrm{III}}(\theta), \tag{25}$$

where G represents the shear modulus, and K_{I}, K_{II} and K_{III} represent the far-field mode I, II and III stress intensity factors, respectively. The dimensionless functions $\tilde{u}_i^{\mathrm{I}}(\theta, \nu)$,

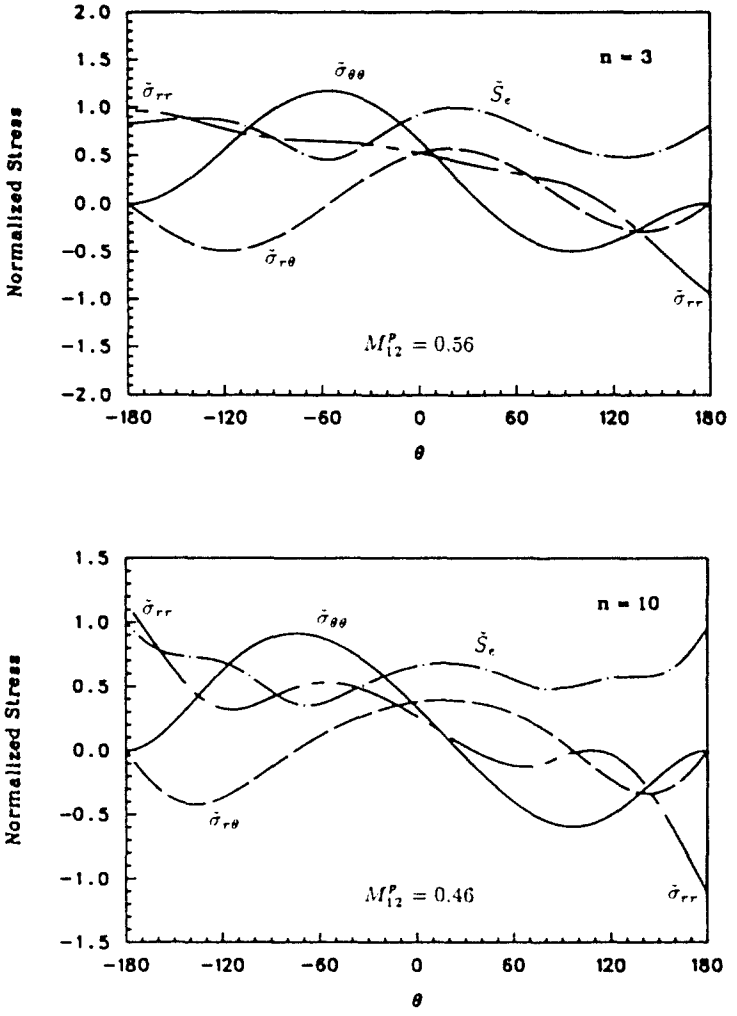

Fig. 2. The normalized angular stress functions of combined mode I and II with the HRR singularity (perturbed from mode III) for (a) $n = 3$, and (b) $n = 10$.

$\tilde{u}_i^{II}(\theta, \nu)$ and $\tilde{u}_3^{III}(\theta)$ are the well-known linear elastic asymptotic displacement solutions [for example, see Kanninen and Popelar (1985)].

The elastic far-field is completely specified by the three stress intensity factors, K_I, K_{II} and K_{III} (recall that the angular functions $\tilde{u}_i^{I}(\theta, \nu)$, $\tilde{u}_i^{II}(\theta, \nu)$ and $\tilde{u}_3^{III}(\theta)$ are known). Alternatively, we can use another set of three parameters, the J integral and two elastic mixity factors, to specify the elastic far-field. The J integral is related to K_I, K_{II} and K_{III} by

$$J = \frac{1-\nu^2}{E}(K_I^2 + K_{II}^2) + \frac{1}{2G}K_{III}^2. \tag{26}$$

The elastic mixity factors M_{13}^e and M_{23}^e related to the mixity of the in-plane modes and the out-of-plane shear mode for the small-scale yielding formulation are defined as

$$M_{13}^e = \frac{2}{\pi}\tan^{-1}\left[\lim_{r\to 0}\frac{\sigma_{\theta\theta}(\theta=0)}{\sigma_{\theta z}(\theta=0)}\right] = \frac{2}{\pi}\tan^{-1}\left[\frac{K_I}{K_{III}}\right] \tag{27}$$

and

$$M_{23}^e = \frac{2}{\pi}\tan^{-1}\left[\lim_{r\to 0}\frac{\sigma_{r\theta}(\theta=0)}{\sigma_{\theta z}(\theta=0)}\right] = \frac{2}{\pi}\tan^{-1}\left[\frac{K_{II}}{K_{III}}\right]. \tag{28}$$

According to eqns (27) and (28), M^{ζ}_{13} and M^{ζ}_{23} equal 0 for pure mode III. When both M^{ζ}_{13} and M^{ζ}_{23} equal 1, a mixity factor M^{ζ}_{12} (Shih, 1973) is required to describe the combined mode I and II crack-tip field,

$$M^{\zeta}_{12} = \frac{2}{\pi}\tan^{-1}\left[\lim_{r\to 0}\frac{\sigma_{\theta\theta}(\theta=0)}{\sigma_{r\theta}(\theta=0)}\right] = \frac{2}{\pi}\tan^{-1}\left[\frac{K_{\mathrm{I}}}{K_{\mathrm{II}}}\right]. \tag{29}$$

The values of M^{ζ}_{13}, M^{ζ}_{23} and M^{ζ}_{12} lie between 1 and 0 for any combination of mode I, II and III loadings. In fact, only two mixity factors are needed to fully describe a mixture of three modes. For a combination involving only two modes, a single mode mixity suffices to quantify the mode mixture. Note that these mixity factors are defined in terms of the relative contributions of the in-plane opening stress, the in-plane shear stress, and the out-of-plane shear stress ahead of the tip. Under small-scale yielding conditions, they can be expressed as functions of the ratios of the stress intensity factors as in (27)–(29).

The finite element model of the circular domain is constructed using 9-node quadrilateral Lagrangian elements. Wedge-shaped 9-node elements are used in the immediate crack-tip region. The size of the wedge-shaped elements in the radial direction is denoted as r_n. These elements are surrounded by circular strips of elements; four strips of elements span each decade of r_n/r_0, where r_0 denotes the radius of the circle as shown in Fig. 1. We take $r_n/r_0 = 10^{-7}$ in this investigation. Therefore, 28 strips of elements, which are generated by a logarithmic scale, span the domain between $r/r_0 = 10^{-7}$ and $r/r_0 = 1$. Within each strip, the angular distance from $-\pi$ to π is spanned by 20 elements of equal size. Therefore, the total number of elements is 580.

The finite element formulation for this work will be discussed only briefly here. The *B-bar* method (Hughes, 1980) is used to construct the strain–displacement matrix of our 9-node quadrilateral Lagrangian elements. This method alleviates the poor performance of our quadrilateral Lagrangian elements in the fully plastic range (Nagtegaal *et al.*, 1974). In this study, we employed the parameter tracking method (Shih and Needleman, 1984). We begin by obtaining the linear elastic solution at a load. This solution is then used as the initial estimate in the iteration for a mildly nonlinear problem with, say, $n = 2$. We then use the convergent solution for the mildly nonlinear problem as the initial estimate for a more nonlinear problem. In this manner, solutions can be obtained for high-hardening to low-hardening materials. Generally speaking, after four to five iterations, a convergent solution, with a Euclidean error norm of about 10^{-6}, for a slightly lower hardening solution is obtained from a slightly higher one.

5. SMALL-SCALE YIELDING NUMERICAL RESULTS

Under combined mode I, II and III loading conditions, the in-plane stresses and out-of-plane shear stresses within the plastic zone are coupled through the effective stress in the plastic stress–strain relations. We have systematically examined the effect of this coupling on near-tip fields. To elucidate the rather complicated nature of the near-tip fields for a complete range of combined-mode loadings, numerical solutions must be presented in an appropriately normalized form. To this end, deformation plasticity solutions for a number of combinations of mode I, II, and III and for hardening exponents n in the range 1–10 are obtained. In these computations, we set $\nu = 0.3$ and $\alpha = 0.1$. Our finite element solutions produced the correct HRR singularities, namely $r^{-1/(n+1)}$, for the special cases of pure mode I, pure mode II, pure mode III and combined mode I and II remote loadings. For the linear elastic problems, the numerical solutions produced the precise elastic $1/\sqrt{r}$ singularity and the associated angular functions for various combinations of mode I, II and III loadings. Furthermore, for each of the convergent solutions, our J values, as calculated by the domain integral method (Li *et al.*, 1985; Shih *et al.*, 1986; Moran and Shih, 1987) for each of the circular strips, differed by less than 1% from the prescribed value as determined by (26). The path-independence of the computed J values and the excellent agreement with (26) attest to the quality of our finite element solutions.

By the process of parameter tracking, we have obtained solutions for the full range of n values ($1 \leqslant n \leqslant 10$) and various mixtures of mode I, II and III. To examine the dependence of the near-tip stresses on the radial distance r (at fixed θ), we plot the normalized stresses as functions of the normalized radial distance to the tip using a log–log scale. The numerically determined stresses are divided by the HRR singularity such that $\tilde{\sigma}_{ij} = \sigma_{ij}/[\sigma_0(J/\alpha\sigma_0\varepsilon_0 r)^{1/(n+1)}]$. The radial distance is normalized by the length of the plastic zone, r_p, at the angle of interest. To examine the angular variations of the near-tip stress fields, we plot the normalized stresses $\tilde{\sigma}_{ij}$ (in the r, θ and z coordinates) as functions of θ at a radial distance of $r/r_p \approx 10^{-3}$. For each problem analysed, the magnitude of the far-field displacement field is chosen so that the maximum extent of the plastic zone (as a function of θ) is no more than 10% of r_0. Thus the stresses deep within the plastic zone can be investigated under the small-scale yielding conditions.

In the interest of space, only solutions for $n = 3$ and 10 and for remote displacement boundary conditions corresponding to three mode mixities are presented. We select the three representative cases where the out-of-plane shear contribution and the in-plane contribution to the remote K fields can be said to be equal to each other. Specifically, we define an equivalent in-plane K parameter, $\bar{K} = (K_I^2 + K_{II}^2)^{1/2}$. The three representative cases have $\bar{K}/K_{III} = 1$. The in-plane mixity factors M^e_{12} of the three cases are varied. They are 0.83, 0.5 and 0.17, which represent $K_{II}/K_I = 0.27$, $K_{II}/K_I = 1$ and $K_I/K_{II} = 0.27$, respectively. The three elastic mixity factors for Case 1 are $M^e_{12} = 0.83$, $M^e_{13} = 0.49$ and $M^e_{23} = 0.16$. The elastic mixity factors for Case 2 are $M^e_{12} = 0.5$, $M^e_{13} = 0.39$ and $M^e_{23} = 0.39$. The elastic mixity factors for Case 3 are $M^e_{12} = 0.17$, $M^e_{13} = 0.16$ and $M^e_{23} = 0.49$.

Figures 3–5 show the normalized in-plane stresses $\tilde{\sigma}_{yy}$, $\tilde{\sigma}_{zz}$, and $\tilde{\sigma}_{xy}$, the normalized

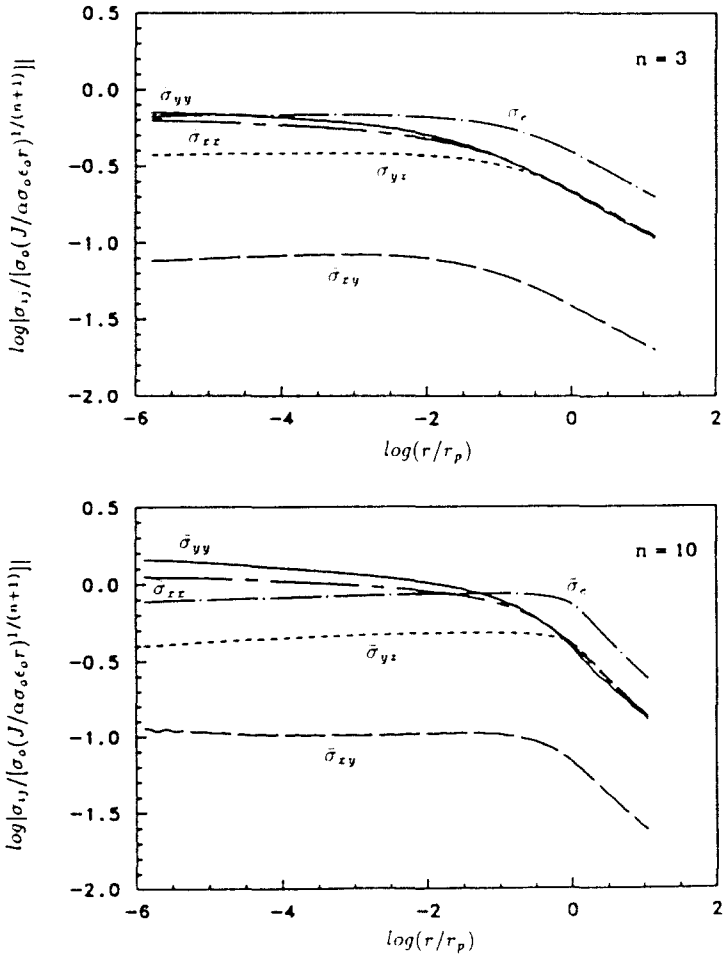

Fig. 3. Case 1 ($M^e_{12} = 0.83$, $M^e_{13} = 0.49$ and $M^e_{23} = 0.16$): the normalized stresses $\tilde{\sigma}_{ij}$ at $\theta = -9$ as functions of r/r_p plotted in a log–log scale for (a) $n = 3$, and (b) $= 10$.

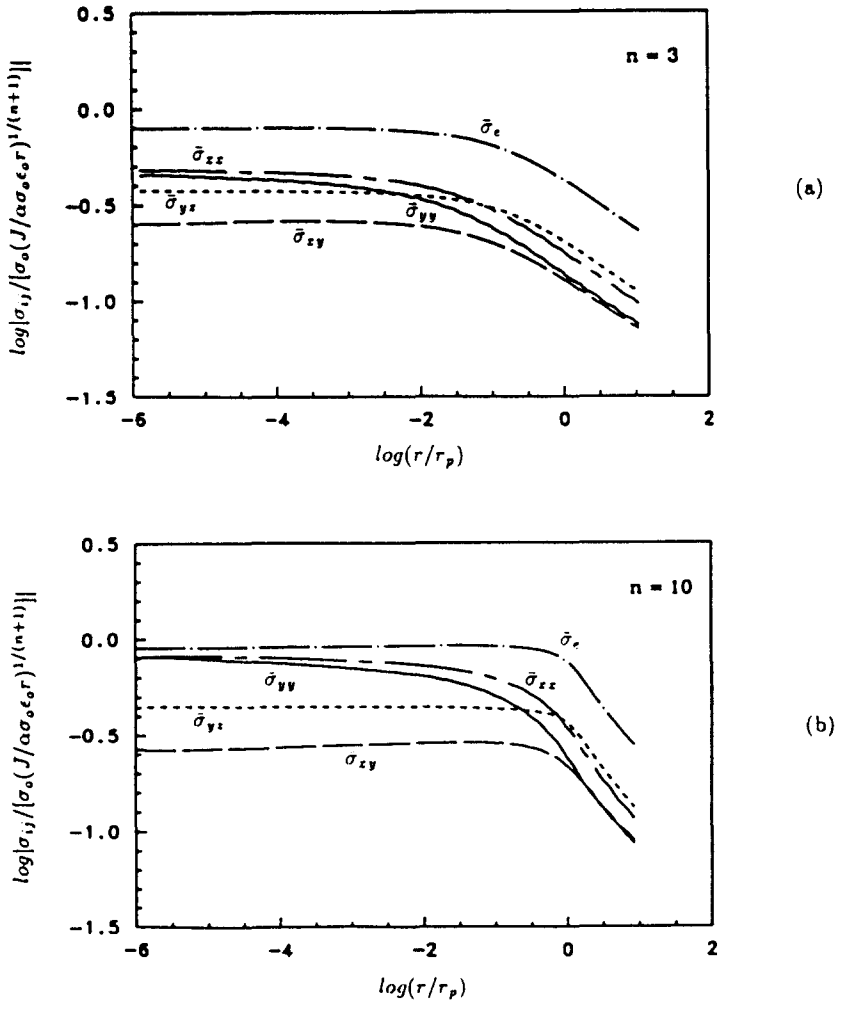

Fig. 4. Case 2 ($M^{\infty}_{12} = 0.5$, $M^{\infty}_{13} = 0.39$ and $M^{\infty}_{23} = 0.39$): the normalized stresses $\tilde{\sigma}_{ij}$ at $\theta = -9^{\circ}$ as functions of r/r_p plotted in a log-log scale for (a) $n = 3$, and (b) $n = 10$.

effective stress $\tilde{\sigma}_e$, and the normalized out-of-plane shear stress $\tilde{\sigma}_{yz}$ at $\theta = -9^{\circ}$ as functions of r/r_p in a log–log scale for Case 1, 2 and 3, respectively. In Figs 3–5, outside of the plastic zone [log $(r/r_p) > 0$], the variation of the stresses with the radial distance is in agreement with the elastic singularity. In general, in Figs 3–5, as r/r_p decreases within the plastic zone, the stresses tend to level off. Since the numerically determined stresses are normalized by the HRR singularity, the levelling-off means the radial variation of the stresses is in accord with the HRR singularity. However, depending upon the mode mixity, the singularities of the stresses may be slightly different from the HRR singularity. In general, the in-plane stresses are more singular than the HRR singularity and the out-of-plane shear stresses are less singular than the HRR singularity when near mode I loading conditions prevail. This effect decreases as the mode II contribution increases.

Figure 3 shows the results for Case 1 where the remote loading has a small mode II contribution and is close to combined mode I and III conditions. The trends of the stress singularities can be seen more clearly for $n = 10$ in Fig. 3b. Deep within the plastic zones, the singularities of the in-plane stresses $\tilde{\sigma}_{xx}$, $\tilde{\sigma}_{yy}$ and $\tilde{\sigma}_{xy}$ are slightly stronger than the HRR singularity and the singularity of the out-of-plane shear stress $\tilde{\sigma}_{yz}$ is slightly weaker than the HRR singularity. However, there is a complicating factor in addition to the coupling effect of the in-plane and out-of-plane shear plastic deformation. Specifically, the asymptotic value of M^{∞}_{12} is larger than the value of M^{∞}_{12} under in-plane mixed-mode conditions (Shih, 1973, 1974). This means that as r decreases, material plasticity enhances the in-plane

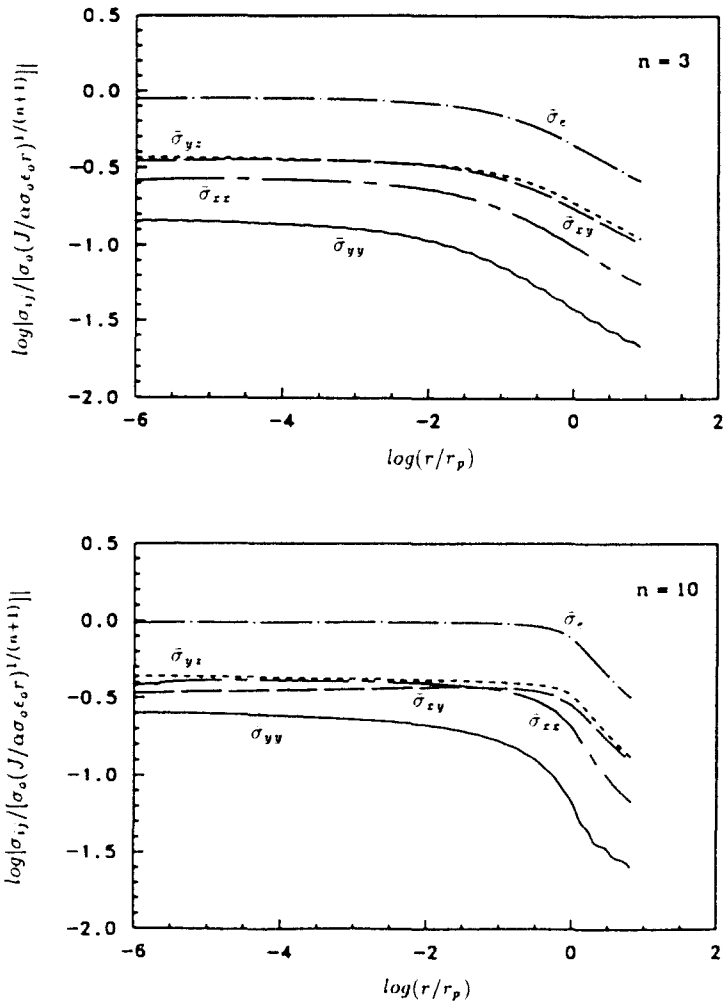

Fig. 5. Case 3 ($M^s_{12} = 0.17$, $M^s_{11} = 0.16$ and $M^s_{21} = 0.49$): the normalized stresses $\tilde{\sigma}_{ij}$ at $\theta = -9$ as functions of r/r_p plotted in a log–log scale for (a) $n = 3$, and (b) $n = 10$.

opening stress relative to the in-plane shear stress ahead of the tip. This effect is more pronounced for low-hardening materials. Here, as r/r_p decreases, $\tilde{\sigma}_{xy}$ for $n = 3$ decreases in Fig. 3a, and $\tilde{\sigma}_{xy}$ for $n = 10$ also decreases initially in Fig. 3b. But as r/r_p further decreases, $\tilde{\sigma}_{xy}$ for $n = 3$ tends to level off in Fig. 3a while $\tilde{\sigma}_{xy}$ for $n = 10$ increases in Fig. 3b. This can be explained by the stronger enhancement of the dominant mode I effects by the presence of mode III loading. Also, low hardening enhances this coupling effect as shown by the larger decrease of $\tilde{\sigma}_{yz}$ for $n = 10$ in Fig. 3b in comparison with that of $\tilde{\sigma}_{yz}$ for $n = 3$ in Fig. 3a as r/r_p decreases.

Solutions for Case 2 where the mode II contribution to the loading is more than that of Case 1 are shown in Fig. 4. All the stresses seem to level off to approach the HRR singularity as r/r_p decreases. However, when we examine the results closely, we find that the singularity of the in-plane shear stress is slightly weaker than the HRR singularity. Figure 5 shows the results for Case 3 where the remote loading has a small mode I contribution and is close to combined mode II and III conditions. In this case, all the stresses seem to level off to approach the HRR singularity as r/r_p decreases. However, when we examine the results closely, we find that the singularity of the in-plane shear stress is slightly weaker than the HRR singularity and the singularity of the out-of-plane shear stress is slightly stronger than the HRR singularity. This trend agrees with that under combined mode II and III conditions.

Figures 6–8 show the normalized stresss $\tilde{\sigma}_{ij}$ at about $r/r_p \approx 10^{-3}$ as functions of θ for Case 1, 2 and 3, respectively. As shown in these figures, and out-of-plane shear stresses $\tilde{\sigma}_{yz}$

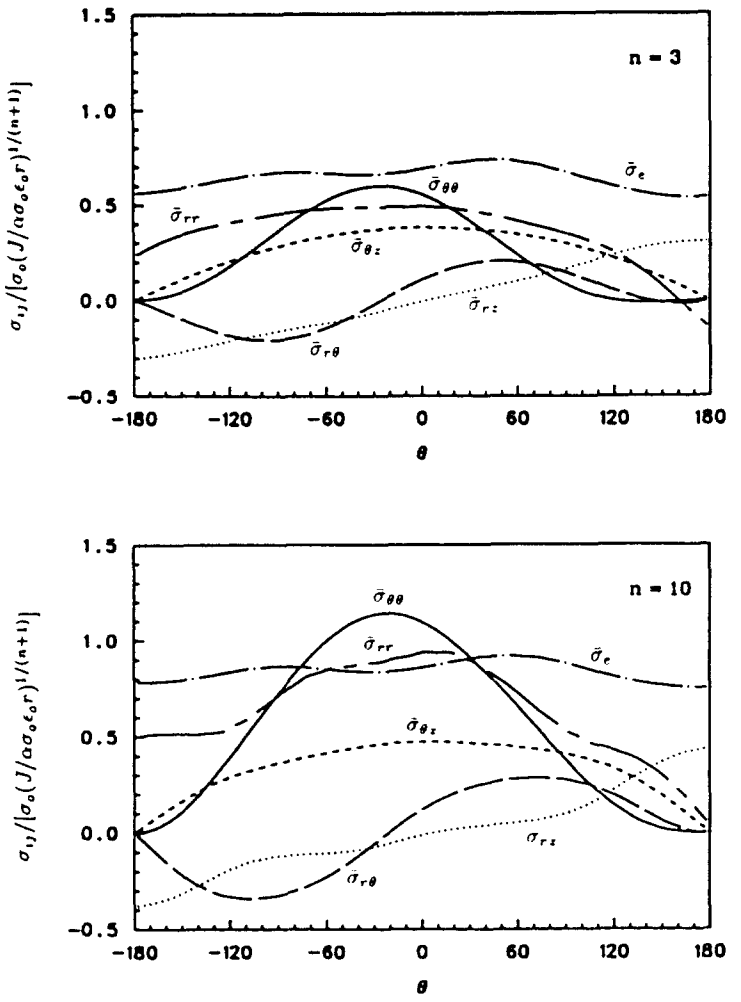

Fig. 6. Case I ($M^e_{12} = 0.83$, $M^e_{13} = 0.49$ and $M^e_{23} = 0.16$): the normalized stresses $\tilde{\sigma}_{ij}$ at $r/r_p \approx 10^{-3}$ plotted as functions of θ for (a) $n = 3$ and (b) $n = 10$.

and $\tilde{\sigma}_{\theta z}$ do not have the anti-symmetry with respect to the crack line due to the coupling effect of the in-plane and out-of-plane shear plastic deformation under asymmetric in-plane loading conditions. Further, these figures show that the elevation of the triaxiality for low-hardening materials (with large n) due to plasticity is higher under near mode I mixed-mode loading conditions. When we compare the angular functions of the in-plane stresses in Figs 6–8 with Fig. 2, we find that the angular functions in Fig. 7a for $n = 3$ with $M^p_{12} = 0.51$ are similar to those in Fig. 2a for $n = 3$ with $M^p_{12} = 0.56$. Also, the angular functions in Fig. 8b for $n = 10$ with $M^p_{12} = 0.33$ are close to those in Fig. 2b for $n = 10$ with $M^p_{12} = 0.46$. These plastic mixity factors are obtained from the stresses at $\theta = 0$, which are interpolated from the finite element results at Gauss points. Under the condition that the values of M^p_{12} are nearly in accord, the qualitative agreement between the angular functions of the full-field finite element results (at a radial distance with a near HRR singularity) and the perturbation solutions with the HRR singularity attests to the quality of both finite element computations. It also provides support for the utility of perturbation analysis to this class of problems to predict the singular behavior of in-plane stresses and out-of-plane shear stresses.

The elastic mixity factors for Case I are $M^e_{12} = 0.83$, $M^e_{13} = 0.49$ and $M^e_{23} = 0.16$. At about $r/r_p \approx 10^{-3}$, the plastic mixity factors are $M^p_{12} = 0.89$, $M^p_{13} = 0.62$ and $M^p_{23} = 0.17$ for $n = 3$ and $M^p_{12} = 0.93$, $M^p_{13} = 0.74$ and $M^p_{23} = 0.16$ for $n = 10$. At about $r/r_p \approx 10^{-5}$, the plastic mixity factors are $M^p_{12} = 0.90$, $M^p_{13} = 0.66$ and $M^p_{23} = 0.17$ for $n = 3$ and $M^p_{12} = 0.94$, $M^p_{13} = 0.79$ and $M^p_{23} = 0.17$ for $n = 10$. These trends of the plastic mixity

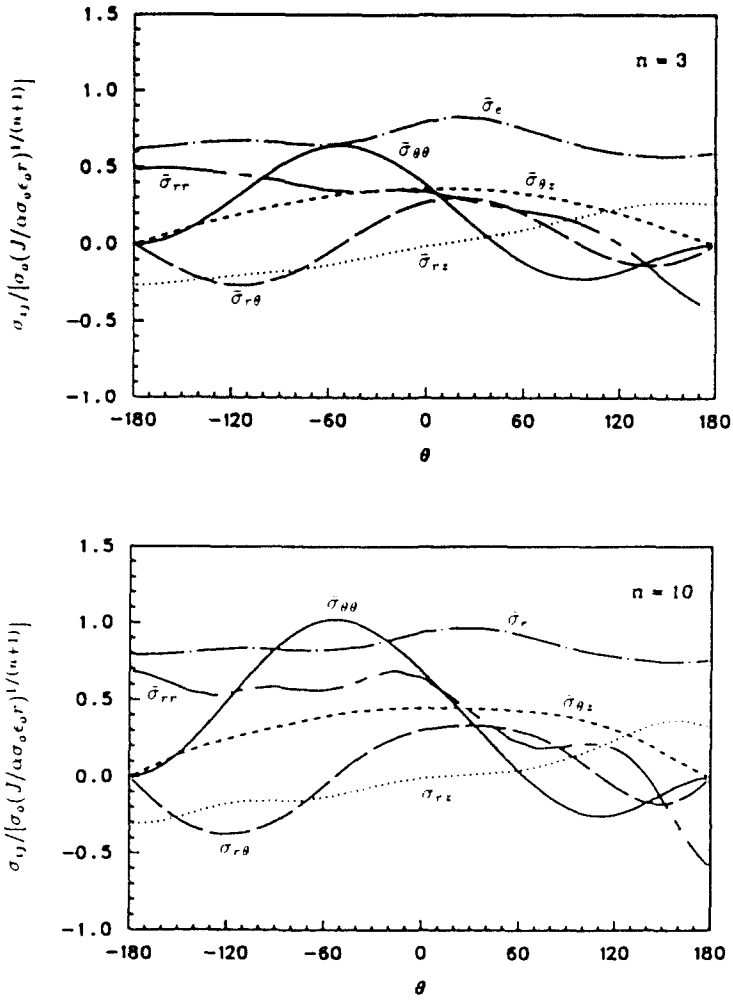

Fig. 7. Case 2 ($M^{\infty}_{12} = 0.5$, $M^{\infty}_{13} = 0.39$ and $M^{\infty}_{23} = 0.39$): the normalized stresses $\tilde{\sigma}_{ij}$ at $r/r_p \approx 10^{-3}$ plotted as functions of θ for (a) $n = 3$ and (b) $n = 10$.

factors continue at a smaller r/r_p. The trends for the three cases are essentially similar: the plastic mixity factors M^{p}_{12} and M^{p}_{13} increase as r/r_p decreases. This effect is more evident for near mode I loading and for low-hardening materials (with large n). The trend of the plastic mixity factor M^{p}_{23} as a function of r/r_p depends upon the competition of the strengthening of the in-plane mode due to the presence of mode I loading and the weakening of the in-plane mode due to the increase of mode II contribution. Low-hardening and near mode I loading promote an increase of M^{p}_{23} as r/r_p decreases. On the contrary, as the mode II contribution increases, as in Case 3, the plastic mixity factor M^{p}_{23} slightly decreases as r/r_p decreases. As we continue to investigate the radial variation of the stresses to very small and physically unreasonable radial distances at $r/r_p \approx 10^{-8}$ for the three cases by using a very refined mesh, the results show that M^{p}_{12} and M^{p}_{13} increases as r/r_p decreases. This suggests that the mode mixtures in Cases 2 and 3 do not have the mathematically exact HRR singularity.

Plastic zones

Figures 9a, b show the plastic zone sizes and shapes for the three cases in the normalized coordinates $\bar{x}$ ($= x\sigma_0^2/JE$) and $\bar{y}$ ($= y\sigma_0^2/JE$) for $n = 3$ and 10, respectively. The normalized plastic zones for the three cases exhibit no symmetry with respect to the crack line; this is similar to those under combined mode I and II conditions but in contrast to those under pure mode I, pure mode II, pure mode III, combined mode I and III and combined mode

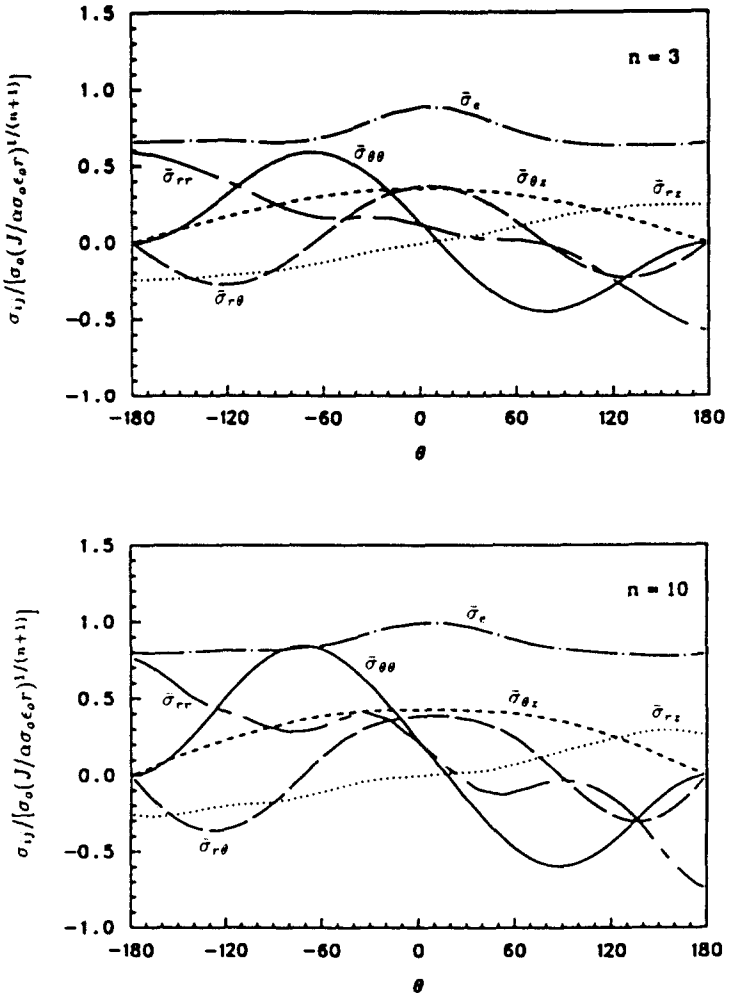

Fig. 8. Case 3 ($M^s_{12} = 0.17$, $M^s_{13} = 0.16$ and $M^s_{23} = 0.49$): the normalized stresses $\bar{\sigma}_{ij}$ at $r/r_p \approx 10^{-3}$ plotted as functions of θ for (a) $n = 3$ and (b) $n = 10$.

II and III conditions. As the mode II contribution increases, the plastic zone becomes increasingly symmetrical with respect to the crack line. The plastic zone shifts ahead of the crack as the hardening exponent n increases. This trend agrees well with those of the pure mode I, pure mode II, pure mode III, combined mode I and II, combined mode I and III, and combined mode II and III cases. Note that the radial extents of the plastic zones as functions of θ for the three cases vary smoothly due to the presence of mode III loading. These features are different from those that develop under pure in-plane loadings but are similar to those for the corresponding combined mode I and III, and combined mode II and III cases.

6. DISCUSSIONS AND CONCLUSIONS

As previously discussed, the in-plane and out-of-plane shear stress and strain fields are coupled through the effective stress. In general, this coupling is rather complex and the stresses for both in-plane and out-of-plane shear modes do not conform to a separable form over distances to the tip which are physically reasonable. However, when either one of the in-plane or out-of-plane shear modes is dominant, the perturbation analysis based on separable stress functions (Pan, 1990) does correctly predict the asymptotic behavior of the full-field solutions (Pan and Shih, 1990a, b). When the contributions of in-plane and out-of-plane shear modes are comparable, no separable asymptotic in-plane and out-of-

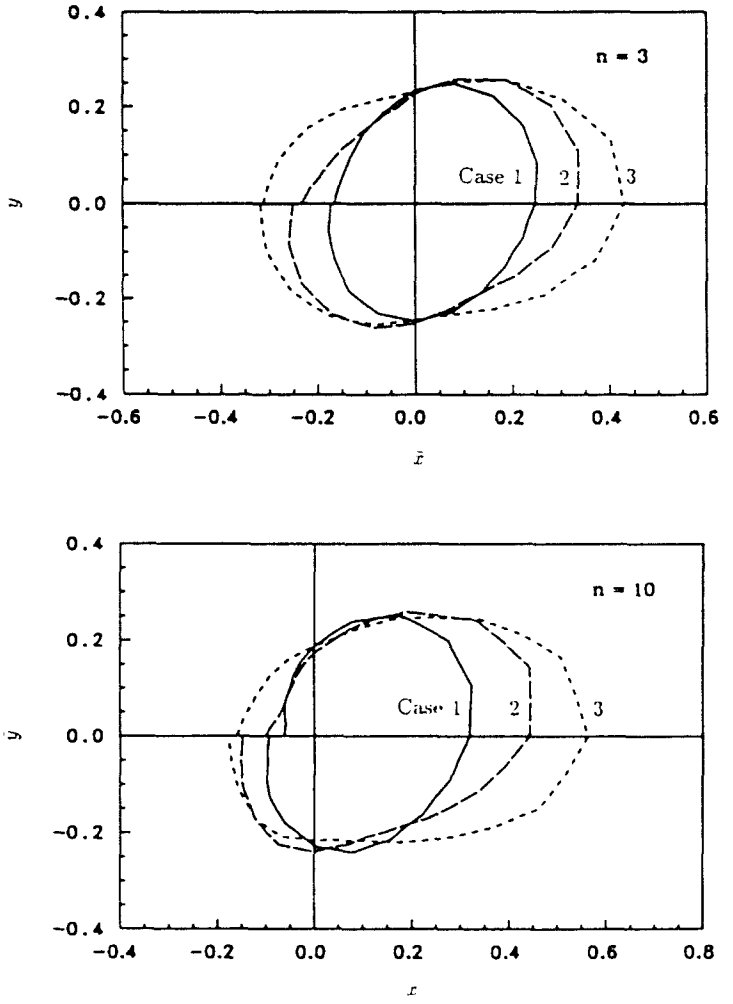

Fig. 9. The plastic zones for Cases 1–3 plotted in the normalized coordinates $\tilde{x}$ (= $x\sigma_0^2/JE$) and $\tilde{y}$ (= $y\sigma_0^2/JE$) for (a) $n = 3$ and (b) $n = 10$.

plane shear stresses are expected except that both in-plane stresses and out-of-plane shear stresses can have the same $r^{-1/(n+1)}$ singularity. Consequently, we do not expect to find the same asymptotic behavior for either the in-plane stresses or the out-of-plane shear stresses at all angles at every mode mixity.

It is an accepted procedure to define mode mixities in terms of the ratios of the in-plane opening stress, in-plane shear stress and the out-of-plane shear stress ahead of the crack. This is the reason for displaying the radial dependencies of the stresses ahead of the tip in Figs 3–5. However these stresses do not provide relative measures of the in-plane versus out-of-plane shear modes when the fields along $\theta \neq 0$ are examined. To carry out comparisons of fields at different angles, it is helpful to use consistent stress quantities representing the out-of-plane and in-plane shear. Consistent stress measures can be derived by considering the effective stress which is an invariant of the deviatoric stress. The effective stress in the cylindrical coordinate system, σ_e, is defined as

$$\sigma_e^2 = \tfrac{1}{2}(\sigma_{rr}-\sigma_{\theta\theta})^2 + \tfrac{1}{2}(\sigma_{\theta\theta}-\sigma_{zz})^2 + \tfrac{1}{2}(\sigma_{zz}-\sigma_{rr})^2 + 3\sigma_{r\theta}^2 + 3\sigma_{rz}^2 + 3\sigma_{\theta z}^2. \tag{30}$$

As in the perturbation analysis, we can define an effective out-of-plane shear stress T_e as

$$T_e^2 = 3\sigma_{rz}^2 + 3\sigma_{\theta z}^2. \tag{31}$$

Note that T_e is an invariant for any coordinate systems rotating with respect to the out-of-plane axis. Then another invariant for these coordinate system rotations can be defined as

$$S_e^2 = \tfrac{1}{2}(\sigma_{rr}-\sigma_{\theta\theta})^2+\tfrac{1}{2}(\sigma_{\theta\theta}-\sigma_{zz})^2+\tfrac{1}{2}(\sigma_{zz}-\sigma_{rr})^2+3\sigma_{r\theta}^2. \tag{32}$$

When the elastic strain is small compared to the plastic strain and can be neglected, eqn (32) reduces to

$$S_e^2 = \tfrac{3}{4}(\sigma_{rr}-\sigma_{\theta\theta})^2+3\sigma_{r\theta}^2 \tag{33}$$

according to plastic incompressibility. By virtue of (33) S_e may be interpreted as an effective in-plane shear stress. Therefore S_e defined in eqn (33) can be regarded as the effective in-plane shear stress. Making use of (31) and (32) we have

$$\sigma_e^2 = T_e^2+S_e^2. \tag{34}$$

The effective out-of-plane plastic shear strain ε_{te} and the effective in-plane plastic shear strain ε_{se} can be defined as

$$\varepsilon_{te} = \alpha\left(\frac{\sigma_e}{\sigma_0}\right)^{n-1}\frac{T_e}{\sigma_0},$$

$$\varepsilon_{se} = \alpha\left(\frac{\sigma_e}{\sigma_0}\right)^{n-1}\frac{S_e}{\sigma_0}. \tag{35}$$

Note that

$$\varepsilon_e^2 = \varepsilon_{te}^2+\varepsilon_{se}^2 = \tfrac{2}{3}\varepsilon_{ij}^p\varepsilon_{ij}^p, \tag{36}$$

where ε_e represents the effective plastic shear strain. Now it is clear from eqn (35) that the ratio T_e/S_e also represents the ratio of the effective plastic shear strains, $\varepsilon_{te}/\varepsilon_{se}$. Therefore the ratio T_e/S_e or parameters based on T_e/S_e can serve to characterize the relative strength of the out-of-plane and in-plane plastic shear for this class of problems. Now we will show that the singularity behaviors of these effective stresses along angles ($\theta = -9^\circ$ and 45°) are consistent for the cases examined in this paper.

In Figs 10a, b, the normalized effective stresses for Case 1 are shown as functions of the normalized radial distance to the tip in a log–log scale for $\theta = -9^\circ$ and 45°, respectively. We present results for $n = 10$ because the low hardening brings out the plasticity effect more vividly. In these plots, the radial distances are normalized by the plastic zone extents at the corresponding angles. The hydrostatic stress σ_h is also plotted to show its singular behavior. In Fig. 10, the general trends of these effective stresses and the hydrostatic stresses relative to the HRR singularity at different angles are consistent: the effective out-of-plane shear stresses have weaker singularities whereas the effective in-plane shear stresses have stronger singularities, the effective stresses have weaker singularities, and the hydrostatic stresses have stronger singularities when compared to the HRR singularity. Note that a field having an HRR singularity exhibits a zero slope in these log–log plots. Upon closer examination we note these effective stresses and the hydrostatic stresses do not have exactly the same slopes at different angles. But the general trends of the singularity behaviors at different angles are consistent. It may be recalled that no consistent trends could be discerned by studying the stress distributions in Fig. 3 where the dominant effect of mode I complicates the stress patterns that develop under Case 1 loading.

For Case 2, the in-plane and out-of-plane shear stresses appear to level off approaching the HRR singularity as r/r_p decreases, as shown in Fig. 4. However, a distinctly different pattern emerges in Figs 11a, b. Here the radial variation of the effective stresses and hydrostatic stress pertaining to Case 2 for $n = 10$ at $\theta = -9^\circ$ and 45° are shown. The effective out-of-plane shear stresses have stronger singularity, the effective in-plane shear

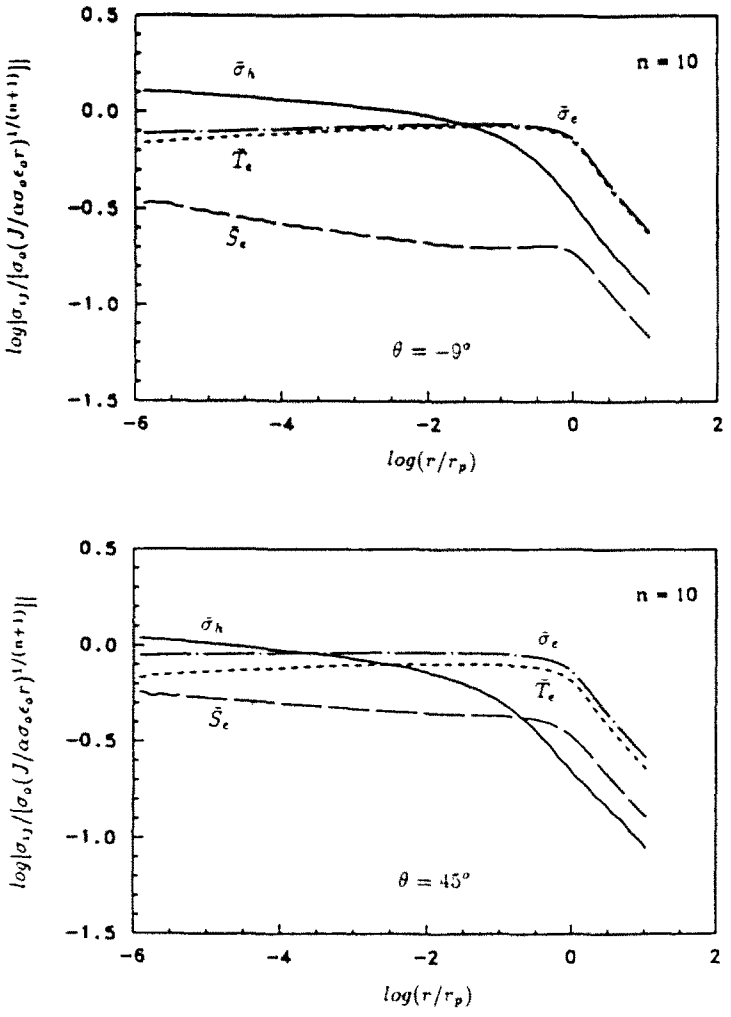

Fig. 10. Case 1 ($M^{\infty}_{12} = 0.83$, $M^{\infty}_{11} = 0.49$ and $M^{\infty}_{23} = 0.16$): the normalized effective stress $\tilde{\sigma}_e$, the normalized effective in-plane shear stress $\tilde{S}_e$, the normalized effective out-of-plane shear stress $\tilde{T}_e$, and the normalized hydrostatic stress $\tilde{\sigma}_h$ for $n = 10$ as functions of r/r_p plotted in a log–log scale at (a) $\theta = -9°$, and (b) $\theta = 45°$.

stresses have weaker singularity, and the hydrostatic stresses have stronger singularity when compared to the HRR singularity. The dominant hydrostatic stress gives the in-plane stresses ahead of the tip with the singularities slightly stronger than the HRR singularity. Strictly speaking, we should regard Case 2 as an out-of-plane shear dominant case under this shear-based plasticity approach. For Case 3 where mode II is dominant, the trend of the singularity behavior of all the effective stresses and the hydrostatic stresses at different angles are the same as those of Case 2. In the interest of space, we do not show the results for Case 3 here. When the mode mixities are defined in the conventional way by the ratios of the in-plane opening stress, in-plane shear stress and out-of-plane shear stress as in eqns (5)–(7), both Cases 2 and 3 can be regarded as in-plane mode dominant cases as r/r_p decreases asymptotically to zero. However, from the shear-based plasticity viewpoint, both Cases 2 and 3 should be regarded as out-of-plane shear dominant cases.

In summary, we have obtained asymptotic solutions of combined mode I and II crack-tip fields perturbed from mode III for cracks in power-law hardening materials. Our solutions indicate that the perturbed combined mode I and II crack-tip fields of certain mode mixities can have the HRR singularity. Our small-scale yielding results show that deep within the plastic zone, under near mode I mixed-mode loadings, the in-plane stresses can be said to be slightly more singular than $r^{-1/(n+1)}$ while the out-of-plane shear stresses

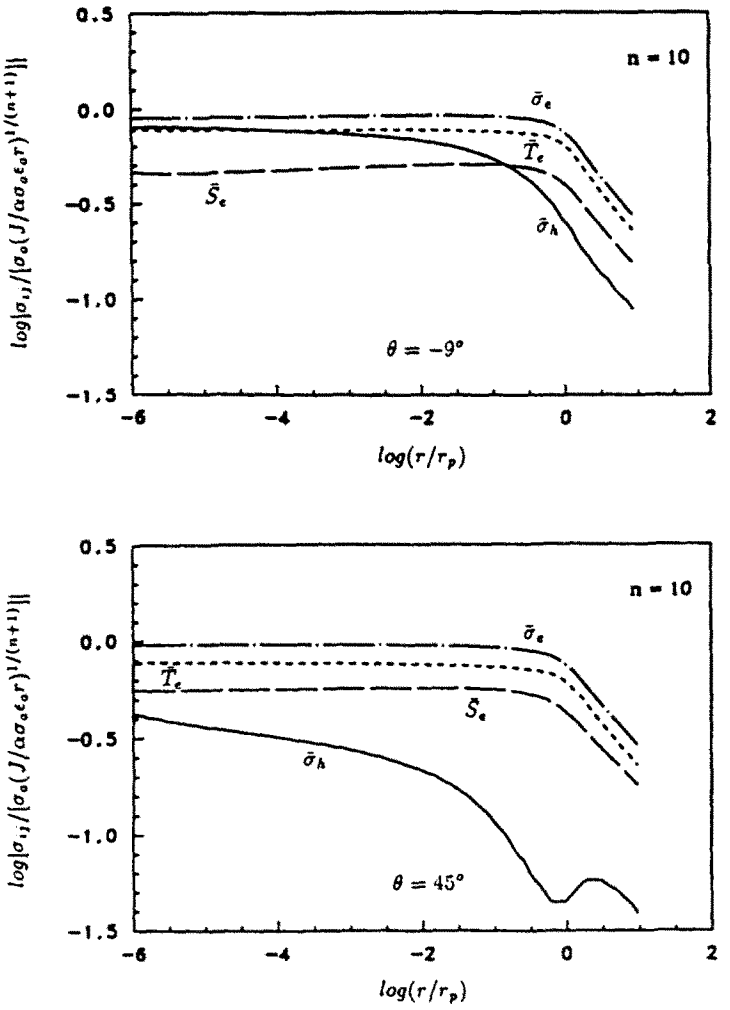

Fig. 11. Case 2 ($M^p_{12} = 0.5$, $M^p_{13} = 0.39$ and $M^p_{23} = 0.39$): the normalized effective stress $\bar{\sigma}_e$, the normalized effective in-plane shear stress $\bar{S}_e$, the normalized effective out-of plane shear stress $\bar{T}_e$, and the normalized hydrostatic stress $\bar{\sigma}_h$ for $n = 10$ as functions of r/r_p plotted in a log–log scale at (a) $\theta = -9°$, and (b) $\theta = 45°$.

are slightly less singular than $r^{-1/(n+1)}$, and the plastic mixity factors M^p_{12} and M^p_{13} increase as r/r_p decreases. The results also demonstrate that the singularities of the in-plane stresses and the out-of-plane shear stresses vary smoothly with mode mixity. Finally, the effective in-plane shear stress and the effective out-of-plane shear stress have been introduced to characterize and quantify the in-plane and out-of-plane shear in a consistent manner for this class of problems.

Acknowledgements—J. P. acknowledges the support of this work by the National Science Foundation under grant No. MSM-8613544 at The University of Michigan. C.F.S. acknowledges the support of this work by the Material Research Group, funded by the National Science Foundation at Brown University. Helpful discussions on this subject with Professor J. R. Rice of Harvard University are greatly appreciated. The reviewer's comments are also appreciated.

REFERENCES

Budiansky, B. and Rice, J. R. (1973). Conservation laws and energy-release rates. *J. Appl. Mech.* **40**, 201–203.

Dong, P. and Pan, J. (1990a). Plane-strain mixed-mode near-tip fields in elastic perfectly plastic solids under small-scale yielding conditions. *Int. J. Fract.* **45**, 243–262.

Dong, P. and Pan, J. (1990b). Asymptotic crack-tip fields for perfectly plastic solids under plane-stress and mixed-mode loading conditions. *J. Appl. Mech.* **57**, 635–638.

Dong, P. and Pan, J. (1990c). Plane-stress mixed mode near-tip fields in elastic perfectly plastic solids. *Engng Fract. Mech.* **37**, 43–57.

Hutchinson, J. W. (1968a). Singular behaviour at the end of a tensile crack in a hardening material. *J. Mech Phys. Solids* **16**, 13–31.

Hutchinson, J. W. (1968b). Plastic stress and strain fields at a crack tip. *J. Mech. Phys. Solids* **16**, 337–347.

Kanninen, M. F. and Popelar, C. H. (1985). *Advanced Fracture Mechanics*. Oxford University Press, Oxford.

Li, F. Z. and Pan, J. (1990a). Plane-strain crack-tip fields for pressure-sensitive dilatant materials. *J. Appl. Mech.* **57**, 40–49.

Li, F. Z. and Pan, J. (1990b). Plane-stress crack-tip fields for pressure-sensitive dilatant materials. *Engng Fract Mech.* **35**, 1105–1116.

Li, F. Z., Shih, C. F. and Needleman, A. (1985). A comparison of methods for calculating energy release rates. *Engng Fract. Mech.* **21**, 405–421.

Moran, B. and Shih, C. F. (1987). Crack tip and associated domain integrals from momentum and energy balance. *Engng Fract. Mech.* **27**, 615–642.

Nagtegaal, J. C., Parks, D. M. and Rice, J. R. (1974). On numerical accurate finite element solutions in the fully plastic range. *Comput. Meth. Appl. Mech. Engng* **4**, 153–178.

Nemat-Nasser, S. and Obata, M. (1984). On stress field near a stationary crack tip. *Mech. Mater.* **3**, 235–243.

Pan, J. (1990). Asymptotic analysis of a crack in a power-law material under combined in-plane and out-of-plane shear loading conditions. *J. Mech. Phys. Solids* **38**, 133–159.

Pan, J. and Shih, C. F. (1986). Plane-strain crack-tip fields for power-law hardening orthotropic materials. *Mech. Mater.* **5**, 299–316.

Pan, J. and Shih, C. F. (1988). Plane-stress crack-tip fields for power-law hardening orthotropic materials. *Int. J. Fract.* **37**, 171–195.

Pan, J. and Shih, C. F. (1990a). Elastic–plastic analysis of combined mode I and III crack-tip fields under small-scale yielding conditions. *J. Mech. Phys. Solids* **38**, 161–181.

Pan, J. and Shih, C. F. (1990b). Elastic–plastic analysis of combined mode II and III crack-tip fields under small-scale yielding conditions. *J. Appl. Mech.* **57**, 259–267.

Rice, J. R. (1968a). A path independent integral and the approximate analysis of strain concentration by notches and cracks. *J. Appl. Mech.* **35**, 379–386.

Rice, J. R. (1968b). Mathematical analysis in the mechanics of fracture. In *Fracture* (Edited by H. Liebowitz), Vol. 2, pp. 191–311. Academic Press, New York, NY.

Rice, J. R. and Rosengren, G. F. (1968). Plane strain deformation near a crack tip in a power law hardening material. *J. Mech. Phys. Solids* **16**, 1–12.

Saka, M., Abe, H. and Tanaka, S. (1986). Numerical analysis of blunting of a crack tip in a ductile material under small-scale yielding and mixed mode loading. *Comput. Mech.* **1**, 11–19.

Shih, C. F. (1973). Elastic–plastic analysis of combined mode crack problems. Ph.D. Thesis, Harvard University, Cambridge, MA.

Shih, C. F. (1974). Small-scale yielding analysis of mixed mode plane-strain crack problems. *Fract. Anal.* ASTM STP **560**, 187–210.

Shih, C. F., Moran, B. and Nakamura, T. (1986). Energy release rate along a three-dimensional crack front in a thermally stressed body. *Int. J. Fract.* **30**, 79–102.

Shih, C. F. and Needleman, A. (1984). Fully plastic crack problems, Parts I and II. *J. Appl. Mech.* **51**, 48–64.

Symington, M., Ortiz, M. and Shih, C. F. (1990). A finite element method for determining the angular variation of asymptotic crack tip fields. *Int. J. Fract.* **45**, 51–64.